CFA/VISHNO 2016

Propagation d'ondes acoustiques dans un milieu périodique avec résonateurs

A. Lardeau[a], J.-P. Groby[b] et V. Romero García[b]
[a]Laboratoire DRIVE-ISAT, 49 rue Mademoiselle Bourgeois, 58027 Nevers Cedex, France
[b]Laboratoire d'Acoustique de l'Université du Maine, Avenue Olivier Messiaen, Cedex9, 72085 Le Mans, France
alexandre.lardeau@u-bourgogne.fr

The propagation properties of a three-dimensional sonic crystal made of square-rod rigid scatterers incorporating a periodic arrangement of quarter wavelength resonators are theoretically and experimentally reported in this work. The periodicity of the system produces Bragg band gaps that can be tuned in frequency by using the orientation of the square-rod scatterers with respect to the incident wave. In addition, the quarter wavelength resonators introduce resonant band gaps that can be tuned by the coupling between the neighbor resonators. Bragg and resonant band gaps can overlap allowing the wave propagation control inside the periodic medium. In particular we experimentally and theoretically show that this system can produce a broad frequency band gap exceeding two and a half octaves (from 590 Hz to 3220 Hz) with transmission lower than 3% in the whole frequency range. Finite element methods are used to calculate the dispersion relation of the locally resonant system. To study the wave propagation in the semi-infinite structures and to compare with the experiments performed in an echo-free chamber, the visco-thermal losses are accounted for in the quarter-wavelength resonators. The numerical predictions are compared with the experimental results measured in an echo free chamber showing good agreement. This work motivates interesting applications of this system as acoustic audible filters.

1 Introduction

Periodic arrays of rigid scatterers embedded in a fluid are the analogues for the acoustic waves of the crystalline structures for the electrons or the photonic crystals for the electromagnetic waves. Such structures are known as Sonic Crystals (SCs) [1] and the exploitation of the periodic distribution of scatterers in such structures have been intensively used to control the acoustic wave propagation. The dispersion relation is governed particularly by both the periodicity and the shape of the scatterers providing different tools to manage the wave propagation. Perhaps the most known property of such systems is the presence of band gaps, ranges of frequencies in which the wave propagation is forbidden. The band gaps appear at high symmetry points in the Brillouin zone due to the presence of a degeneracy of the band structure produced by the Bragg interferences at frequencies in the diffractive regime ($\lambda \simeq a$, λ being the wavelength of the incident wave and a the lattice constant characterizing the periodicity of the structure). Many interesting physical phenomena arise from this particular dispersion relation such as wave localization [2], excitation of evanescent waves [3], as well as relevant applications concerning filtering [4] and wave guiding [5]. In particular, many approaches have been proposed to lift the band degeneracy and thus enlarge the band gaps [6]. Some possibilities consist of either reducing the total symmetry of the crystal in order to remove some band degeneracies, allowing the appearance of complete gaps [7] or optimizing the shape of the scatterers [8].

Interesting properties can be obtained in the low frequency regime ($\lambda << a$) in periodic structures if local resonators are used as scatterers. In acoustics, the pioneering works of Bradley [10] and Sugimoto [11] theoretically and experimentally examined the propagation of sound waves in a waveguide loaded periodically with local resonators (quarter-wavelength and Helmholtz resonators). In these systems two different mechanisms are responsible to the generation of band gaps. In addition to the Bragg interferences producing the band gap due to the periodicity, the resonance produces an other band gap when the frequency of sound waves coincides with the natural frequency of the resonators, producing a hybridization between the resonance and the dispersion of the non resonant periodic structure. This fact has been used to introduce the concept of acoustic metamaterials with resonant band gaps at low frequencies, orders of magnitude smaller than the Bragg band gap [12, 13], as well as to improve the absorption capabilities of porous materials in the low frequency regime [14].

In this article we exploit the idea of the direct coupling of the local resonant scatterers to generate multiple resonances that can be combined with the effect of periodicity in order to produce a broadband frequency region with high transmission loss. We experimentally and theoretically study the propagation properties of a three-dimensional SC made of square-rod rigid scatterers incorporating a periodic arrangement of quarter wavelength resonators. Particularly, we analyze different configurations in which the indirect coupling between the resonators in the structure generates multiple resonances that are designed to be close to the Bragg band gap. The combined effect produces an overlap of the stop bands that can be used to strongly reduce the transmission in a broadband range of frequencies. In particular, we experimentally and theoretically show that the system can produce a broad frequency band gap exceeding two and a half octaves (from 590 Hz to 3220 Hz) with transmission lower than 3% in the whole range. Finite element methods are used to study the dispersion relation of the locally resonant system. To study the wave propagation in the semi-infinite structures and to compare with the experiments performed in an echo-free chamber, the visco-thermal losses are accounted for in the quarter-wavelength resonators.

2 Experimental set-up

The resonant scatterers are square-rod scatterers made of wood (acoustically rigid for the ranges of frequencies analyzed in this work) with side length l having a 1D periodic array of quarter wavelength resonators incorporated in one of its faces, with periodicity a_z. The quarter wavelength resonators are made by drilling cylindrical holes of radius R and length L in one of the faces of the square rod scatterer. The resonant square rod scatterers are placed in a square array of periodicity a. Figure 1(a) shows the scheme of the resonant square rod scatterer showing the parameters of the unit cell of the crystalline structure analyzed in this work. Figure 1(b) shows the scheme of the finite array analyzed in this work as well as a picture of the SC in the anechoic chamber. As shown in the inset of the Fig. 1(b) the unit cell can be rotated by an angle θ with respect to the center of the resonant square rod scatterer, adding a degree of freedom to manage the dispersion relation of the system.

The experimental prototype consists of a 14×6 array,

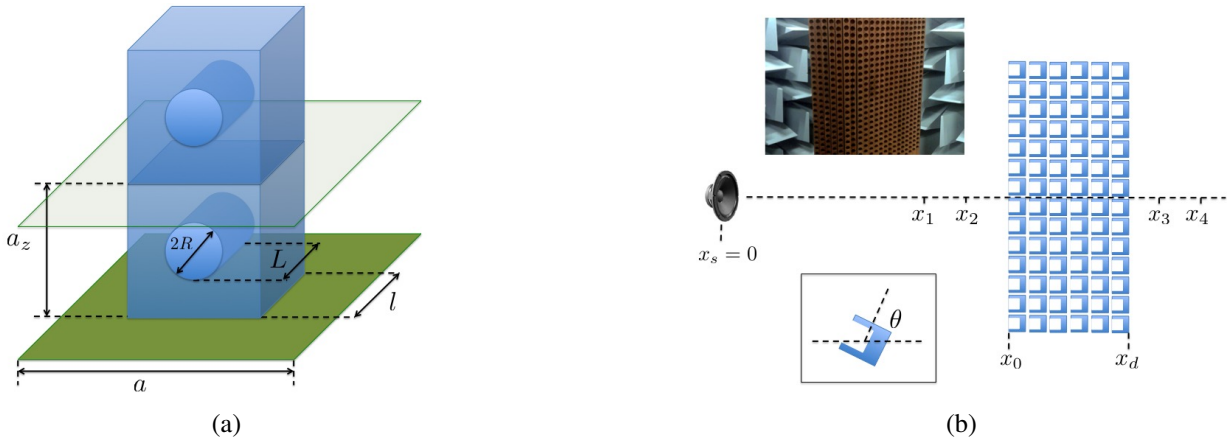

(a) (b)

Figure 1 – (a) Scheme of the resonant square-rod scatterer showing two unit cells. The horizontal planes delimit the bounds of the unit cell. (b) Scheme of the finite SC made of N rows of scatterers. Four points, x_i with ($i = 1, 2, 3, 4$), are used to evaluate the transfer matrix elements. The insets represent a picture of the SC in the anechoic chamber used in the experimental characterization and the definition of the angle of rotation of the unit cell, θ, with respect to the x-axis.

located on a square lattice with constant $a = 7.5$ cm with a vertical periodicity of the quarter wavelength of $a_z = 5$ cm. The scatterers have a side length $l = 5$ cm. The quarter wavelength resonator has a radius $R = 3.5$ cm and length $L = 4$ cm. The scatterers are 2 m long.

All the acoustic measurements are performed using a microphone B&K 1/4" type 4135. The acoustic source was the loudspeaker Genelec 8351A. The movement of the microphone in the anechoic chamber is controlled by a 1D robotized arm (Zaber LSQ) designed to move the microphone over a 1D trajectory in steps of 1 cm. The acquisition of the acoustic signal is done using the Stanford SR 785 analyzer. The movement of the robotized arm and the acquisition are synchronized by a computer. Once the robotized system is turned off, the acoustic source generates a swept sine signal and the microphone detects it. The analyzer provides the frequency domain signals (module and phase for each frequency).

In the approach considered here, a loudspeaker placed in $x_s = 0$ was used to generate the acoustic field in the anechoic chamber, and a single microphone was used to measure the transfer functions between the signal provided to the loudspeaker and the sound pressure at the four locations shown in Fig. 1(b). Those transfer functions are denoted P_1 to P_4. The loudspeaker is placed far enough from the SC, so that the wave front is considered plane, however, we have to consider that the amplitude of the wave decays as $1/\sqrt{x_i}$ where x_i is the distance between the loudspeaker and the i-th location of the microphone. For the present purposes P_1 to P_4 may be considered to represent the complex sound pressure at the four measurement locations x_1 to x_4, i.e.,

$$P_1 = A\frac{e^{-\imath kx_1}}{\sqrt{x_1}} + B\frac{e^{\imath kx_1}}{\sqrt{x_1}}, \qquad P_2 = A\frac{e^{-\imath kx_2}}{\sqrt{x_2}} + B\frac{e^{\imath kx_2}}{\sqrt{x_2}},$$
$$P_3 = C\frac{e^{-\imath kx_3}}{\sqrt{x_3}} + D\frac{e^{\imath kx_3}}{\sqrt{x_3}}, \qquad P_4 = C\frac{e^{-\imath kx_4}}{\sqrt{x_4}} + D\frac{e^{\imath kx_4}}{\sqrt{x_4}}. \qquad (1)$$

Here, k represents the wave number in the ambient fluid and $e^{+\imath\omega t}$ sign convention has been adopted ($\omega = 2\pi f$ is the angular frequency with f the frequency). The four complex pressures, P_1 to P_4, comprise various superpositions of positive- and negative-going waves in the up- and downstream segments of the anechoic chamber; the complex amplitudes of those waves are represented by the coefficients A to D. Equations (1) yield four equations for the coefficients A to D in terms of the four measured sound pressures, i.e.,

$$A = \frac{\imath(\sqrt{x_1}P_1e^{\imath kx_2} - \sqrt{x_2}P_2e^{\imath kx_1}))}{2\sin(k(x_1 - x_2))},$$
$$B = \frac{\imath(\sqrt{x_2}P_2e^{-\imath kx_1} - \sqrt{x_1}P_1e^{-\imath kx_2}))}{2\sin(k(x_1 - x_2))},$$
$$C = \frac{\imath(\sqrt{x_3}P_3e^{\imath kx_4} - \sqrt{x_4}P_4e^{\imath kx_3}))}{2\sin(k(x_3 - x_4))},$$
$$D = \frac{\imath(\sqrt{x_4}P_4e^{-\imath kx_3} - \sqrt{x_3}P_3e^{-\imath kx_4}))}{2\sin(k(x_3 - x_4))}. \qquad (2)$$

The latter coefficients provide the input data for subsequent transfer matrix calculations. Here, the transfer matrix is used to relate the sound pressures and normal acoustic particle velocities on the two faces of the SC respectively located at x_0 and x_d as in Fig. 1(b), i.e.,

$$\begin{bmatrix} P \\ V \end{bmatrix}_{x_0} = \begin{bmatrix} T_{11} & T_{12} \\ T_{21} & T_{22} \end{bmatrix} \begin{bmatrix} P \\ V \end{bmatrix}_{x_d}. \qquad (3)$$

In Eq. (3), P is the exterior sound pressure and V is the exterior normal acoustic particle velocity. The pressures and particle velocities on the two surfaces of the SC may easily be expressed in terms of the positive- and negative-going wave component amplitudes, i.e.,

$$P(x_0) = \frac{Ae^{-\imath kx_0} + Be^{\imath kx_0}}{\sqrt{x_0}}, \qquad V(x_0) = \frac{Ae^{-\imath kx_0} - Be^{\imath kx_0}}{\sqrt{x_0}\,\rho c},$$
$$P(x_d) = \frac{Ce^{-\imath kx_d} + De^{\imath kx_d}}{\sqrt{x_d}}, \qquad V(x_d) = \frac{Ce^{-\imath kx_d} - De^{\imath kx_d}}{\sqrt{x_d}\,\rho c}. \qquad (4)$$

where ρ is the ambient fluid density and c is the ambient sound speed. Thus, when the plane wave components are known based on measurements of the complex pressures at four locations, the pressures and the normal particle velocities at the two surfaces of the SC can be determined.

It is then of interest to determine the elements of the transfer matrix since, as will be shown below, the elements of that matrix may be directly related to the properties of the SC. Then, instead of making a second set of measurements

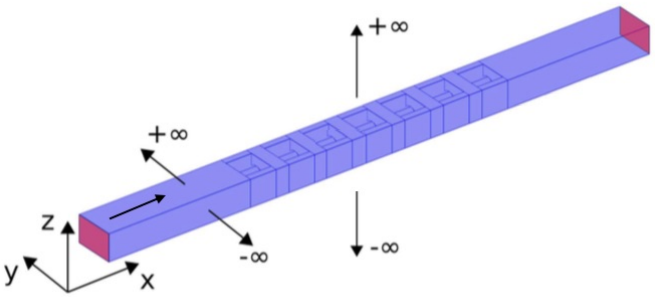

Figure 2 – Semi infinite slab of $N = 7$ resonators. Periodic boundary conditions are considered in the y and z directions while PML conditions are considered in the boundaries of the x direction. A plane wave impinges the slab from the negative values of the x-axis.

it is possible to take advantage of the reciprocal nature of the SC. Thus, given reciprocity and symmetry, it follows that

$$T_{11} = T_{22}, \tag{5}$$

$$T_{11}T_{22} - T_{12}T_{21} = 1. \tag{6}$$

Then, the transfer matrix elements can be expressed directly in terms of the pressures and velocities on the two surfaces of the SC. Therefore, if the transmission coefficient is defined as $T = C/A$, and we consider anechoic termination, $D = 0$, it can be expressed in function of the elements of the transfer matrix

$$T = \frac{2\sqrt{x_d}e^{\imath k(x_d - x_0)}}{(\sqrt{x_0}(T_{11} + T_{12}/(\rho c) + (\rho c)T_{21} + T_{22}))}. \tag{7}$$

3 Numerical characterization

Due to the complexity of the geometry of the resonant square-rod scatterers we choose numerical methods to solve both the eigenvalue and the scattering problems. The Finite Elements Method (FEM) is used for this purpose. Therefore it is necessary to define the symmetry, discretize the domain and consider the boundary conditions for each configuration. In the following subsections we will give the details for each configuration. In a general way, we discretize the domains at least with 10 points for the minimal analyzed wavelength, λ_{min}. The study has been performed in a range of normalized frequencies, fa/c, from 0 to 0.8, therefore $\lambda_{min} = 0.8a$.

3.1 Eigenvalue problem

The eigenvalue problem is solved to obtain the dispersion relation of the periodic medium. The problem $\omega(k)$ is solved using only the unit cell of the crystal and applying the Floquet-Bloch periodic conditions. The properties of the Bloch states constrain the solution to a unit cell with Bloch vectors in the first Brillouin zone. The unit cell is shown in Fig. 1(a). Neumann boundary conditions, representing rigid walls, are considered on the walls of the scatterer. In the entrance of the quarter wavelength resonator the continuity of the pressure and velocity are imposed. By fixing the wavevector, k, in the irreducible Brillouin zone of the unit cell we can obtain the eigenfrequencies for each wave vector. These features transform the unit cell in a bounded domain to solve the problem with the next boundary condition at the borders of the unit cell

$$p(\vec{r} + \vec{R}) = p(\vec{r})e^{\imath\vec{k_B}\vec{R}}, \tag{8}$$

where $\vec{R}$ is the lattice vector and k_B is the Bloch vector that scans the first irreducible Brillouin zone. In our work, the unit cell is a cubic one, therefore $\vec{R} = (na\vec{u_x} + ma\vec{u_y} + la_z\vec{u_z}$. In this work we will not consider the effect in the z-direction, therefore we study the dispersion relation considering the variation of the $k_{Bx} = [0, \pi/a]$ and $k_{By} = [0, \pi/a]$ in the first irreducible zone of Brillouin of a cubic lattice having $k_{Bz} = 0$.

3.2 Scattering problem

Considering the wave propagation in free space (unbounded acoustic domain) the assumption that no waves are reflected from infinity is taken. This is known as the Sommerfeld condition. The solutions of exterior Helmholtz problems that satisfy the Sommerfeld conditions are called radiating solutions. Using FEM it is only possible to obtain some approximation of the radiating solutions in unbounded domains by applying some artificial boundaries in the numerical domain. We use the perfectly matched layers (PML) technique to this purpose.

The geometry considered in this work is shown in Fig. 2. We considered a semi-infinite slab made of N resonators; periodic boundary conditions are used in the y and z directions therefore the structure is infinite in y and z directions but finite in the x one. A plane wave impinges the structure from the negative x-axis and the PML condition is considered at the apendicular x-domain in the extremes of the domain in the x direction to numerically reproduce the Sommerfeld condition in this direction. The acoustic field will be evaluated in the yx-plane, crossing the unit cell in the middle of resonator.

The losses in the quarter-wavelength resonators are taken into account by considering the Zwikker and Kosten model [15], which provides the expression for the equivalent density and bulk modulus in the cylindrical tube of radius R as,

$$\rho_{eq} = \frac{\rho}{1 - 2(-\imath\omega/\nu)^{-1/2}G\left(R(-\imath\omega/\nu)\right)^{1/2}/R}, \tag{9}$$

$$K_{eq} = \frac{\gamma P_0}{1 - 2(\gamma - 1)(-\imath\omega/\nu')^{-1/2}G\left(R(-\imath\omega/\nu')\right)^{1/2}/R}, \tag{10}$$

where $\nu = 1.47\ 10^{-5}$ m^{2}s^{-1} is the kinematic viscosity of air, ω is the angular frequency of the wave, $\nu' = 2.22\ 10^{-5}$ is the

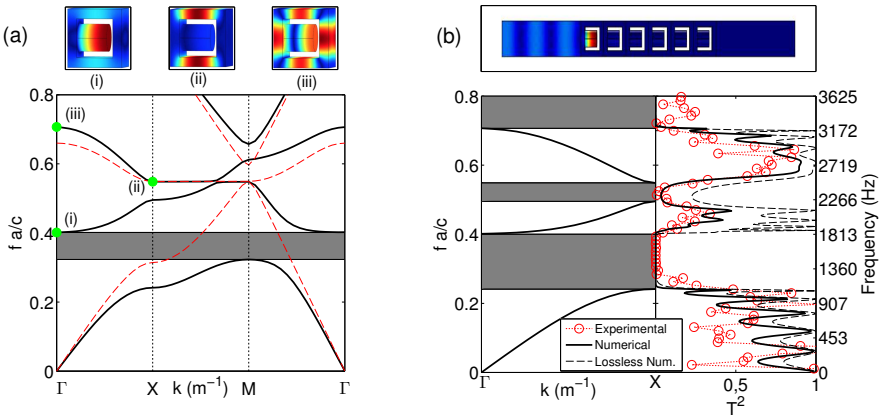

Figure 3 – Characterization of the locally resonant SC with the scatterers placed with $\theta = \pi/2$. (a) shows the dispersion relations for the resonant SC (—) in comparison with the ones without the quarter-wavelength resonator, i.e., just square-rod scatterers (- - -). Gray area represents the full band gap opened by the presence of the resonators in the SC. Insets (i), (ii) and (iii) represents the eigenvectors at frequencies shown in the dispersion relation with the dots. (b) Upper panel represents the solutions of the numerical predictions for the scattering problem at the resonant frequency of the quarter-wavelength resonators. Left panel represents the dispersion relation in the ΓX direction. Gray areas represent the pseudo band gaps at this normal incidence. Right panel represents the transmission coefficient of a finite slab made of 6 rows of resonant square rods. Continuous (Dashed) line represents the numerical predictions with (without) losses in the resonators. Open circles represent the experimental measurement.

thermal diffusivity of air, and the function $G(x)$ is defined as,

$$G(x) = \frac{J_1(x)}{J_0(x)}, \tag{11}$$

where J_n is the Bessel function of $n-$th order and first kind.

4 Results

Before studying the periodic structures, we start by analyzing the transmission through one row of resonant square rod scatterer with $\theta = \pi/2$. This will allow us to characterize the resonant frequency of the quarter-wavelength resonator. Figure 4(a) shows the transmission coefficient, T^2, for this system. Numerical simulations with and without losses in the resonators are plotted using continuous and dashed black lines respectively. Red open circles show the measured transmission coefficient. The minimum of transmission appears at the resonant frequency of the quarter-wavelength resonators. In fact, if we numerically evaluate the acoustic pressure field at this frequency, $fa/c = 0.3824$, we can observe [see Fig. 4(b)] that the resonance is activated and the acoustic field is mostly localized in the resonators. Notice that for this configuration the effect of the losses is not so much sensitive, however, we maintain the presence of losses because, as we will see later, this effect is not negligible when increasing the number of resonators.

4.1 Single resonant SC made of square-rod scatterers with quarter wavelengths resonators

The dispersion relation numerically obtained for a SC made of resonant square rods with $\theta = \pi/2$ is shown in Fig. 3(a) with black lines. In order to compare with the non resonant case, we have represented the band structures for the same square rods without the quarter wavelength

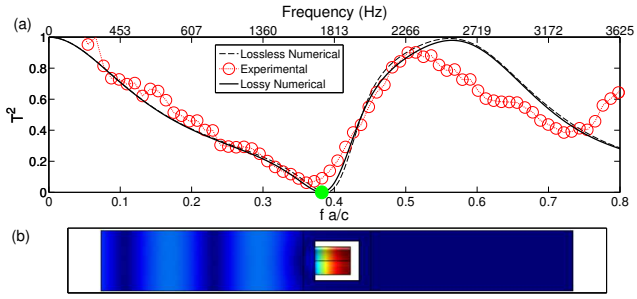

Figure 4 – Characterization of a row of resonant square rod scatterers with $\theta = \pi/2$. (a) Transmission coefficient, T^2, of a row of resonant square rod scatterer. Continuous (Dashed) line represents the numerical predictions with (without) losses in the resonators. Red open circles represent the experimental measurement obtained with the method explained in Section 2. Big dot represents the numerical value of the transmission coefficient at the resonant frequency of the quarter-wavelength resonators, $fa/c = 0.3824$. (b) Pressure field numerically obtained by solving the scattering problem, as shown in Section 3, at the resonance frequency of the quarter wavelength resonators.

resonators (red lines)[9]. While the non resonant structure does not present full band gaps, the SC with the resonant square rod scatterers presents a full band gap [gray area in Fig. 3(a)] around the resonant frequency of the quarter-wavelength resonators, due to the hybridization of the resonance with the background medium.

If we pay attention to the ΓX direction, i.e., normal to the SC interface as it is plotted in Fig. 1(b) three band gaps are present [see Fig. 3(b)]. The first one due to the hybridization band around the resonant frequency of the quarter wavelength resonators; the second one is produced by the Bragg interferences inside the SC due to the periodicity around $fa/c = 0.5$; and the third one is produced by the coupling of the second Bragg band gap and the second resonant mode of the resonators [see the eigenvector (iii) in

Fig. 3(a)].

The transmission coefficient is evaluated for a slab made of 6 rows of resonant square rod scatterers with $\theta = \pi/2$. The results are plotted in the right panel of Fig. 3(b). The three stop bands are well recognized both numerically and experimentally in the transmission coefficient. We would like to notice here the effect of the losses due to the visco-thermal effect in the quarter-wavelength resonators. Black continuous line represents the numerical transmission coefficient with losses, while the dashed line without. As predicted in previous works [16, 17], the effect of losses is more important in the regions with high dispersion and small group velocity. In our problem, the values of the transmission with losses is reduced more than a half around these particular regions. From now on, all the numerical results concerning the transmission coefficient will consider the losses.

4.2 Multi-resonant SC made of square-rod scatterers with quarter wavelengths resonators

Using the degree of freedom given by the rotation of the resonant scatterers we can evaluate a configuration which consists of facing four different resonant square rod scatterers as shown in Fig. 5. The direct coupling between the resonators allows the system to produce additional resonances in the range of frequencies of interest, which introduce more band gaps in the dispersion relation and broaden the range of frequencies with no transmission through the structure.

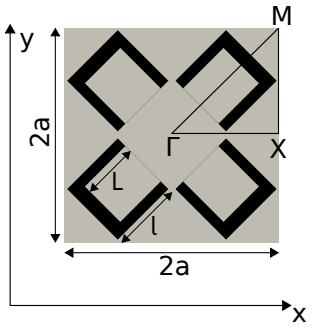

Figure 5 – Unit cell facing four different resonant square rod scatterers.

Figure 6 shows the numerical predictions and experimental results for the configuration facing four neighbor resonant square rod scatterers. Figure 6(a) shows the dispersion relation of such a periodic distribution. Seven full band gaps are opened in this configuration. Different kind of phenomena are mixed in this system. On one hand, as in the previous structures, the periodicity opens band gaps due to Bragg interferences as for example the first and second band gaps around the eigenvector (i) [see the Fig. 6(b)], and the resonances of quarter wavelength resonators open band gaps due to this resonance, for example around the frequency of the eigenvector (iv). However, the interest of such configuration is the direct coupling between the four scatterers. This opens resonant band gaps at frequencies different from those of an isolated quarter wavelength resonator. For example, band gaps around the frequencies of the eigenvectors (iii) and (v) are results of this phenomenon. This concentration of band gaps in the range of frequencies of interest can be used to produce a broad band of low transmission.

The transmission through a finite structure made of three unit cells of four faced resonant square rod scatterers (total $N = 6$ resonant square rod scatterers in the x-direction) is analyzed in the right panel of Figure 6(a). In the numerical simulations, continuous line, we observe that the band gaps predicted by the eigenvalue problem are reproduced in the transmission. Moreover, the effect of the losses in the resonators destroys the transmission peaks that should be produced by the flat bands in the dispersion relation. As previously mentioned, the flat bands having a small group velocity and high dispersion, are strongly affected by the presence of losses in the system, destroying any propagation around this areas. Experimentally, the transmission coefficient also reproduces the band gaps predicted by these eigenvalue problem in agreement with the numerical evaluation of the transmission coefficient. The slightly differences between the experimental results and the numerical ones, can be due to the presence of additional losses in the system, as for example those coming from the viscothermal losses produced between the walls of the resonant square rod scatterers that are not considered in this work. Regarding the transmission of this system, we can see that the combined effect of periodicity and coupled resonators produces an overlap of the band gaps that can be used to strongly reduce the transmission in a broadband range of frequencies. In particular we experimentally and theoretically show that the system can produce a broad frequency band gap exceeding two and a half octaves, from 590 Hz to 3220 Hz, with transmission lower than 3% in the whole range.

5 Conclusions

In this work we use acoustic waves to experimentally prove the physical properties of modulated resonant systems made of resonant square-rod scatterers as well as to design broadband or selective filtering of acoustic waves. Extensive simulations and experimental results in order to show tunable transmission properties of arrays made of resonant square-rod scatterers embedded in air are performed here. We have experimentally and theoretically shown that by rotating some of the resonant square-rod scatterers of a square array, one can easily activate the coupling between them producing additional band gaps in the dispersion relation as well as modifying the Bragg interferences. The combined effect of the periodicity and the coupled resonances produces an overlap of the stop bands that can be used to strongly reduce the transmission in a broadband range of frequencies. In particular, we experimentally and theoretically show that the system can produce a broad frequency band gap exceeding two and a half octaves (from 590 Hz to 3220 Hz) with transmission lower than 3% in the whole range. This work could also be effectively extended to progressing toward the realization of tunable systems for light, liquid, and other waves, which will lead to great potential in ultrasonics for example. The tunability we demonstrated in this work could be applied to control not only the band gap but other properties of the system.

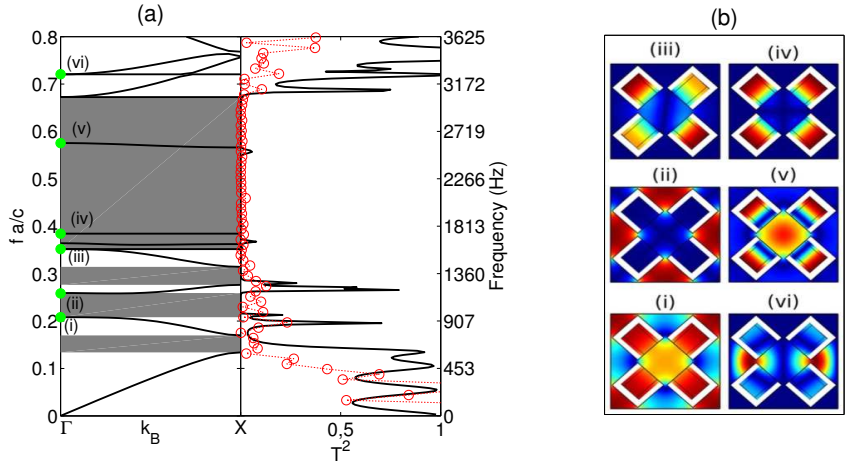

Figure 6 – Characterization of the configuration with four face to face quarter wavelength. (a) Left panel represents the dispersion relation in the Γ*X* direction. Gray areas represent the pseudo band gaps in this incidence. Right panel represents the transmission coefficient of a finite slab made of 6 rows of resonant square rods. Continuous line represents the numerical predictions with losses in the resonators. Open circles represent the experimental measurement. (b) Panels representing the eigenvectors at frequencies shown in the dispersion relation (left panel of (a)) with the dots.

Acknowledgments

This work has been funded by the Metaudible project ANR-13-BS09-0003, co-funded by ANR and FRAE.

References

[1] R. Martínez-Sala, J. Sancho, J. V. Sánchez, V. Gómez, J. Llinares & F. Meseguer, *Sound Attenuation by sculpture*, Nature 378, 241 (1995).

[2] M. Sigalas, *Elastic wave band gaps and defect states in two-dimensional composites*, J. Acoust. Soc. Am., 101, 1256, (1997).

[3] V. Romero-García, J. V. Sánchez-Pérez, S. Castiñeira-Ibáñez & L. M. Garcia-Raffi, *Evidences of evanescent Bloch waves in Phononic Crystals*, Appl. Phys. Lett., 96, 124102, (2010).

[4] V. Sánchez-Morcillo, K. Staliunas, V. Espinosa, I. Pérez-Arjona, J. Redondo & E. Soliveres, *Propagation of sound beams behind sonic crystals*, Phys. Rev. B, 80, 134303 (2009).

[5] V. Romero-García, J. Vasseur, L. M. Garcia-Raffi & A. C. Hladky-Hennion, *Theoretical and experimental evidence of level repulsion states and evanescent modes in sonic crystal stubbed waveguides*, New J. Phys., 14, 023049, (2012).

[6] D. Caballero, J. Sánchez-Dehesa, C. Rubio, R. Martínez-Sala, J. Sánchez-Pérez, F. Meseguer & J. Llinares, *Large two-dimensional sonic band gaps*, Phys. Rev. E, 60, R6316, (1999).

[7] M. Kushwaha, P. Halevi, L. Dobrzynski & B. Djafari-Rouhani, *Acoustic Band Structure of Periodic Elastic Composites*, Phys. Rev. Lett., 71, 2022–2025, (1993).

[8] C. Goffaux, J. P. Vigneron, *Theoretical study of a tunable phononic band gap system*, Phys. Rev. B, 64, 075118, (2001).

[9] V. Romero-García, C. Lagarrigue, J. P. Groby, O. Richoux & V. Tournat, *Tunability of band gaps and waveguides in periodic arrays of square-rod scatterers: Theory and experimental realization*, J. Phys. D: Appl. Phys, 46, 305108, (2013).

[10] C. E. Bradley, *Acoustic Bloch wave propagation in a periodic waveguide*, Texas Univ At Austin Applied Research Labs, (1991).

[11] N. Sugimoto & T. Horioka, *Dispersion characteristics of sound waves in a tunnel with an array of Helmholtz resonators*, J. Acoust. Soc. Am., 97, 1446, (1995).

[12] Z. Liu, X. Zhang, Y. Mao, Y. Zhu, Z. Yang, C. Chan & P. Sheng, *Locally Resonant Sonic Materials*, Science, 289, 1734, (2000).

[13] N. Fang, D. Xi, J. Xu, M. Ambati, W. Srituravanich, C. Sun & X. Zhang, *Ultrasonic metamaterials with negative modulus*, Nature Materials, 5, 452–456, (2006).

[14] J. P. Groby, B. Nennig, C. Lagarrigue, B. Brouard, O. Dazel & V. Tournat, *Enhancing the absorption properties of acoustic porous plates by periodically embedding Helmholtz resonators*, J. Acous. Soc. Am., 137, 273–280, (2015).

[15] C. Zwikker & C. Kosten, *Sound absorbing materials*, Elsevier Publishing Company, New-York, (1949).

[16] A. Duclos, D. Lafarge & V. Pagneux, *Transmission of acoustic waves through 2D phononic crystal: visco-thermal and multiple scattering effects*, Eur. Phys. J. Appl. Phys., 45, 11302, (2009).

[17] G. Theocharis, O. Richoux, V. Romero-García & V. Tournat, *Slow sound propagation in lossy locally resonant periodic structures*, New J. Phys., 16, 093017, (2014).